Journal of Crystal Growth 477 (2017) 183–187

Contents lists available at ScienceDirect

Journal of Crystal Growth

journal homepage: www.elsevier.com/locate/crys

Stencil lithography of superconducting contacts on MBE-grown topological insulator thin films

Peter Schüffelgen [a,*], Daniel Rosenbach [a], Elmar Neumann [a], Martin P. Stehno [b], Martin Lanius [a], Jialin Zhao [c], Meng Wang [c], Brendan Sheehan [d], Michael Schmidt [d], Bo Gao [c], Alexander Brinkman [b], Gregor Mussler [a], Thomas Schäpers [a], Detlev Grützmacher [a]

[a] Peter Grünberg Institut, Forschungszentrum Jülich & JARA Jülich-Aachen Research Alliance, D-52425 Jülich, Germany
[b] MESA+ Institute for Nanotechnology, Interfaces and Correlated Electrons, University of Twente, 7500AE Enschede, The Netherlands
[c] State Key Laboratory of Functional Materials for Informatics, Shanghai Institute of Microsystem and Information Technology, Chinese Academy of Sciences, Shanghai 200050, China
[d] Tyndall National Institute, University College Cork, Lee Maltings, Dyke Parade, Cork T12 R5CP, Ireland

ARTICLE INFO

Article history:
Available online 23 March 2017
Communicated by Jean-Baptiste Rodriguez

Keywords:
B2. Topological insulator
B2. Superconductor
B3. Josephson junction
A3. Molecular beam epitaxy
A1. Shadow mask
A1. Stencil lithography

ABSTRACT

Topological insulator $(Bi_{0.06}Sb_{0.94})_2Te_3$ thin films grown by molecular beam epitaxy have been capped in-situ with a 2 nm Al film to conserve the pristine topological surface states. Subsequently, a shadow mask - structured by means of focus ion beam - was in-situ placed underneath the sample to deposit a thick layer of Al on well-defined microscopically small areas. The 2 nm thin Al layer fully oxidizes after exposure to air and in this way protects the TI surface from degradation. The thick Al layer remains metallic underneath a 3–4 nm thick native oxide layer and therefore serves as (super-) conducting contacts. Superconductor-Topological Insulator-Superconductor junctions with lateral dimensions in the nm range have then been fabricated via an alternative stencil lithography technique. Despite the in-situ deposition, transport measurements and transmission electron microscope analysis indicate a low transparency, due to an intermixed region at the interface between topological insulator thin film and metallic Al.

1. Introduction

Three-dimensional (3D) topological insulators (TIs) possess an insulating bulk and metallic surface states with their spin locked to the momentum [1,2]. In proximity to an s-wave superconductor (SC), quasi-particle excitations – so called Majorana zero modes (MZMs) – are predicted to occur at the surface of TIs [3]. Due to their non-abelian exchange statistics, such MZMs are expected to enable fault-tolerant quantum computation [4,5]. While the final proof for their existence is still elusive, first signatures of Majorana Modes have been found in 3D and 2D HgTe topological insulator thin films [6,7]. HgTe is known for its very distinctive surface transport and low bulk carrier contribution [8]. However, its small bandgap of about 10 meV makes any application based on the topological surface states impossible for room temperature devices. In contrast, $(Bi_{0.06}Sb_{0.94})_2Te_3$ TI thin films have a sufficiently large bandgap of about 200 meV [9]. Unfortunately Bi-Sb based topological insulator thin films suffer from high bulk carrier contributions, which make the observation of surface transport in magnetoelectric measurements challenging [10]. Several attempts have been made to reduce bulk carrier concentration and increase surface mobility [11–13].

In 2012 Lang et al. reported for the first time, how an AlO_x capping layer can effectively preserve the pristine surface states from degradation [14]. Before exposing the sample to air, the authors deposited 2 nm of Al on top of the TI surface. The Al film immediately oxidized after taking the sample to ambient conditions, forming a native oxide, which prevents the topological insulator from oxidation and effectively preserves surface transport. Transferring this technique from widely separated contacts for magneto-transport experiments to Josephson junctions (JJs), having contacts separated only tens to hundreds of nm, lead to first signatures of 4π-periodic Josephson supercurrents in $(Bi_{0.06}Sb_{0.94})_2Te_3$ thin films [15]. Crucial for this observation is an interface without any barrier between TI and SC [16]. Therefore, the rather robust AlO_x capping

Abbreviations: TI, topological insulator; SC, superconductor; JJ, Josephson junction; MZM, Majorana zero mode; MBE, molecular beam epitaxy; QL, quintuple layer; S-TI-S, Superconductor-Topological Insulator-Superconductor; TEM, transmission electron microscope; vdW, van-der-Waals.

* Corresponding author.
E-mail addresses: p.schueffelgen@fz-juelich.de (P. Schüffelgen), g.mussler@fz-juelich.de (G. Mussler).

http://dx.doi.org/10.1016/j.jcrysgro.2017.03.035
0022-0248/

needs to be removed thoroughly in the contact area. Due to possible damage or oxygen inclusion in the TI surface during removal of AlO_x, the TI-SC interface transparency is affected. Consequently, inducing a robust supercurrent in AlO_x-capped TIs is challenging [17].

To solve this problem, we made use of stencil lithography [18]. This technique allows one to cap the topological insulator in-situ, and also enables one to deposit superconducting contacts without breaking the vacuum via shadow mask growth. A thin Si-membrane has been patterned by focused ion beam (FIB). The obtained shadow mask with lateral dimensions in the μm range allows one to grow a thick Al film (50 nm) on well-defined microscopically small areas on top of a previously deposited macroscopically large thin Al layer (2 nm), leaving two differently thick Al-layers on top of the TI thin film. After exposure to air, the thin Al layer completely oxidizes, forming the protective insulating capping, while the thick layer serves as metallic contacts.

2. Sample preparation

The topological thin film was grown by molecular beam epitaxy (MBE) on n-type doped Si:P(1 1 1) substrate (>2000 Ω cm), which was wet chemically cleaned by a RCA HF-last procedure. The dip in 1% HF passivates the surface during ex-situ transport to the MBE growth chamber. After removing the hydrogen passivation at 700 °C for 10 min under UHV conditions, the substrate temperature was set to 300 °C. Knudsen effusion cell temperatures were then set to their operating temperatures (Bi = 450 °C, Sb = 450 °C and Te = 330 °C) for evaporation. Bi_2Te_3, Sb_2Te_3 as well as ternary compounds $(Bi_{1-x}Sb_x)_2Te_3$ of those two materials grow on Si (1 1 1) in a rhombohedral structure [19,20]. Five atomic layers thereby form a so-called quintuple layer (QL). Within these five layers Bi/Sb and Te bonds are found to be covalent, while in between two QLs a van-der-Waals (vdW) gap is present. The Sb and Bi concentrations of the 30 nm thick $(Bi_{1-x}Sb_x)_2Te_3$ thin film amount to 6% (Bi) and 94% (Sb), respectively (schematically in Fig. 1a). For this composition, the Fermi level is as close as 2 ± 7 meV with respect to the Dirac point [21]. Detailed growth parameters, structural analysis and electrical characterization of such ternary compounds are presented elsewhere [10]. After cooling down the substrate to −30 °C, the Al effusion cell is ramped up to 1100 °C. At this temperature, the Al deposition rate amounts to 7 nm/h. Thin films of Al grown on top of the (0 0 0 1) surface of rhombohedral $(Bi_{0.06}Sb_{0.94})_2Te_3$ are polycrystalline. Grains crystallize in fcc structure, preferably in the (1 1 1) orientation. The Al shutter was opened for 17 min to deposit a layer of 2 nm Al in-situ on top of the ternary compound to cover the delicate topological surface states (Fig. 1b). Subsequently, the shadow mask was placed around 500 μm beneath the sample in-situ, and another 50 nm of Al was deposited while the substrate rotation was turned off (Fig. 1c). In this manner, the pattern of the shadow mask was transferred on top of the heterostructure, comprised of 30 nm TI and 2 nm metallic Al. The thin Al layer (dark) will oxidize completely in air, whereas the thick layer (bright areas) remain metallic and only the top 3–4 nm will form a native oxide once the sample is taken out of the vacuum (Fig. 1d). The contacts pads are arranged in a way that in between them a Hall bar structure

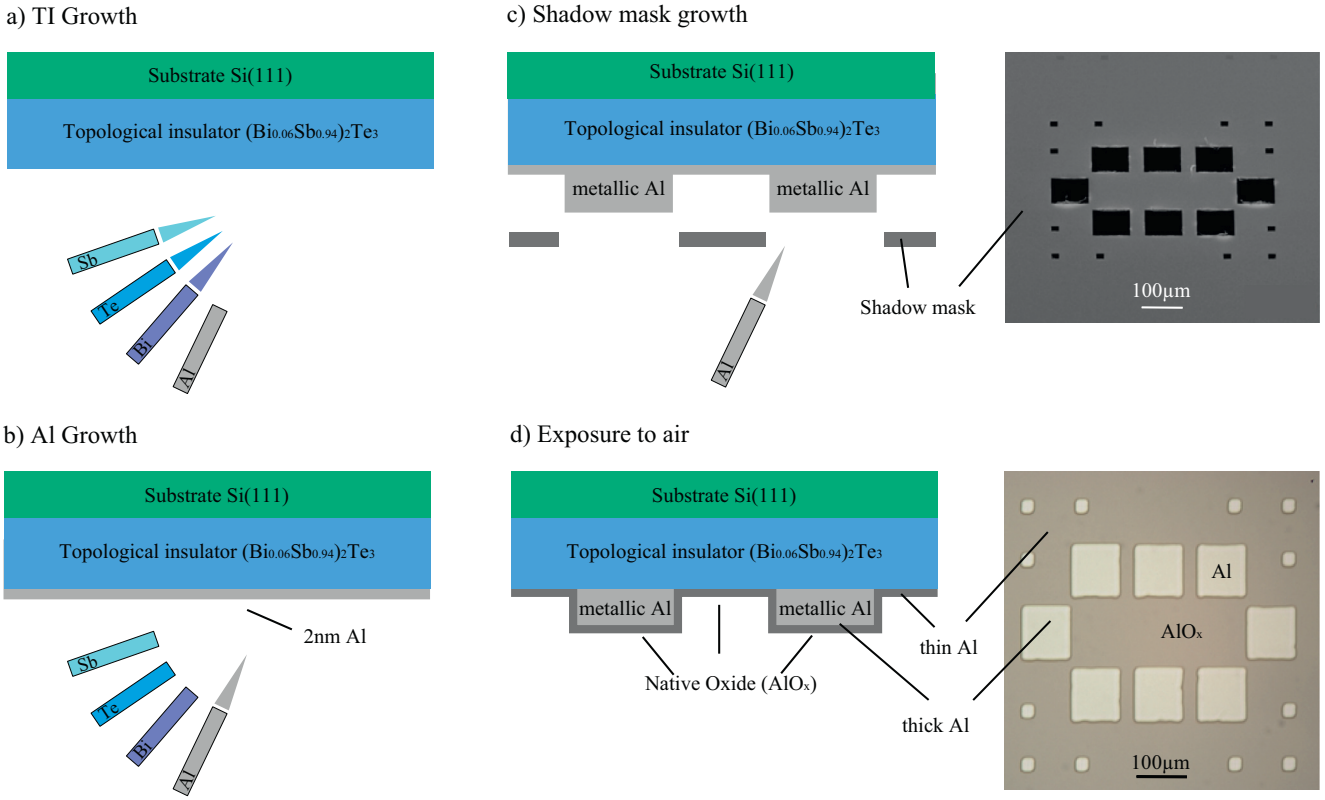

Fig. 1. Stencil Lithography. (a) Growth of the 30 nm TI thin film. (b) Deposition of 2 nm Al on the entire wafer. (c) A shadow mask is placed approximately 500 μm under the thin film via a home-build in-situ transfer system. A second layer of Al then grows selectively. (d) After exposing the sample to air, the thin Al fully oxidizes. The 50 nm thick Al forms a native 3–4 nm thick AlO_x protection layer, while close to the interface of the TI metallic Al should still be present.

can be defined via ion beam etching in a next fabrication step. To align the Hall bar layout to the contact pads by electron beam lithography (EBL) the grown EBL markers in the corners of the sample can be used.

3. Shadow mask fabrication

Single crystalline silicon membranes have been purchased from Norcada Inc. [22]. Photo in Fig. 2a shows an example of such a membrane. The frame (purple) has the dimensions of $10 \times 10\ mm^2$ and a thickness of 500 µm. The membrane (yellow) itself is $4 \times 4\ mm^2$ in size and only 200 nm thick. The surface of the membrane is in (100) plane. By defining rectangular structures, the FIB will cut along crystallographic axes. Patterns were fabricated via a FEI Helios NanoLab DualBeam FIB into the silicon membrane (Figs. 1c and 2b). The smallest structures are separated by freestanding silicon bridges, which have widths down to 100 nm (Fig. 2c). While large structures (Fig. 1c) are beneficial for in-situ grown Hall bar devices, the nanometer-wide bridges can be used for the fabrication of in-situ deposited JJs. As soon as the contacts are separated by only several tens to hundreds of nm from each other, a supercurrent may be induced across the junction. For fabrication of such small structures by stencil lithography one needs to bring mask and sample in close proximity [18]. Since we could not place our mask close enough to the surface of the sample, an alternative stencil lithography technique has been used to define closely separated contacts for the characterization of the SC-TI interface.

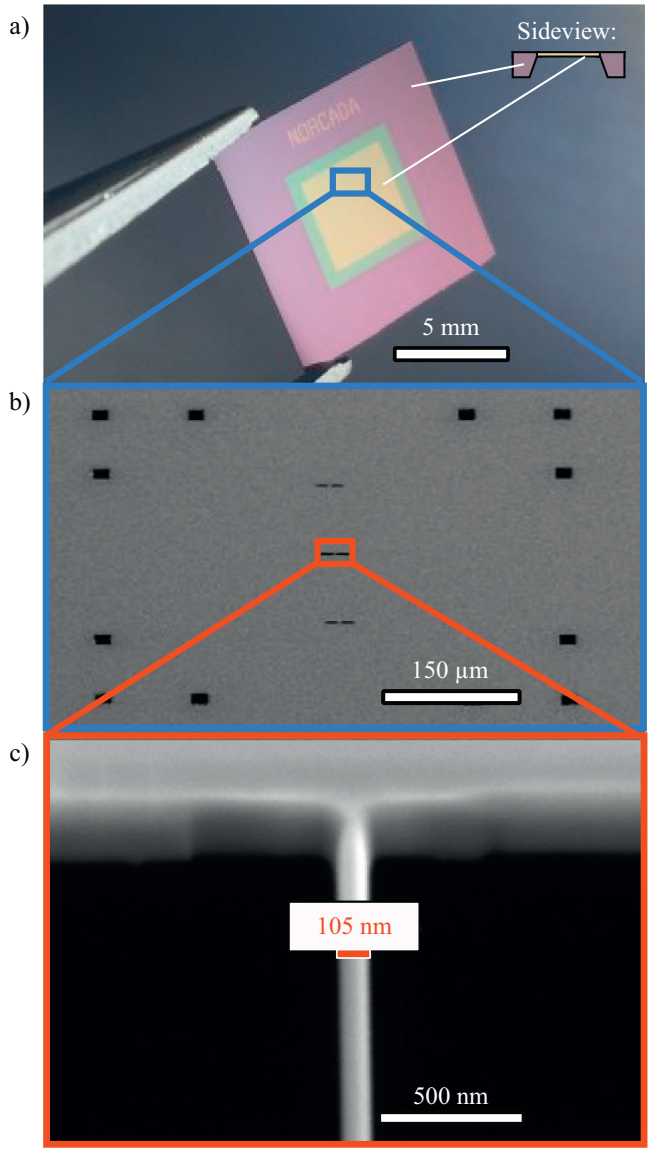

Fig. 2. Shadow mask. (a) A commercially available Si membrane from Norcada company has a $4 \times 4\ mm^2$ Si membrane in the center of the chip. The membrane is only 200 nm thick (yellow) and is surrounded by a stabilizing 500 µm thick frame (purple). Adapted from Ref. [22]. (b) Structures of different dimensions have been defined by FIB. Device contacts are seen in the center of the membrane. EBL markers for further ex-situ fabrication are visible in the corners. (c) Lateral structures as narrow as 100 nm have been fabricated. (For interpretation of the references to colour in this figure legend, the reader is referred to the web version of this article.)

4. Al - $(Bi_{0.06}Sb_{0.94})_2Te_3$ interface

Superconductor - Topological Insulator - Superconductor (S-TI-S) junctions were consisted of Al evaporated via shadow mask on top of an Al-capped $(Bi_{0.06}Sb_{0.94})_2Te_3$ thin film. By making use of an alternative stencil lithography technique,[1] we successfully fabricated grown S-TI-S junctions with a contact separation below 100 nm (Fig. 3a). In a next step, the differential resistance of one junction was measured for low temperatures within an Oxford Triton dilution refrigerator. The junction did not enter the superconducting regime. Instead, the differential resistance across the junction ($R_{S\text{-}TI\text{-}S}$) increased, while cooling down to 25 mK (Fig. 3b). We carried out magnetic-field-dependent measurements at 25 mK and 1.25 K (Fig 2c). At 25 mK we see a pronounced zero magnetic field peak, indicating a low interface transparency. As soon as the magnetic field increases, the differential resistance decreases rapidly. We observe a minimum symmetrically at around ±15 mT, indicating the critical field of the Al. As soon as the magnetic field exceeds the critical field, the resistance increases again with the Al now in the normal conducting state. At 1.25 K, the zero magnetic field peak and its characteristic slope is still visible, but much less pronounced, due to the lower pairing energy at higher temperatures. This feature is typical for superconducting contacts on topological insulator thin films with a low interface transparency [23]. To further investigate the quality of the interface we carried out transmission electron microscope (TEM) studies with a JEOL 2100 HR-TEM on a thin film comprised of 30 nm Al on top of 25 nm $(Bi_{0.06}Sb_{0.94})_2Te_3$. In the lower part of Fig. 3 d) single QLs and adjacent vdW gaps are visible. At the interface to the metallic Al film, one can clearly discern an intermixed region of around 3 nm. This interlayer and the signatures in magneto transport indicate the formation of a barrier due to interdiffusion. The intermixing will also take place at the interface to the thin Al layer between the thick Al contacts. XPS measurements confirmed oxygen incorporation throughout the thin Al-layers after exposure to air (data not shown). TEM analysis (not shown) and electronic transport measurements [14] confirmed native AlOx layers to successfully protect the underlying topological insulator thin films from oxygen incorporation. The combination of MBE and stencil lithography holds the potential of UHV-fabrication of pristine topological Josephson junctions in the nm range with a high throughput. With this method, common problems and limits of EBL, like residual resist-sidewalls, or oxidation during ex-situ fabrication are circumvented [24,25]. An additional thin layer of W, Pt or Ti in the contact area between TI and thick Al might reduce interdiffusion and improve the SC-TI interface transparency. As soon as the material issues have been clarified and the interface quality

[1] Since this technique is still in the process of being patented, details about it are confidential and therefore not discussed in this work.

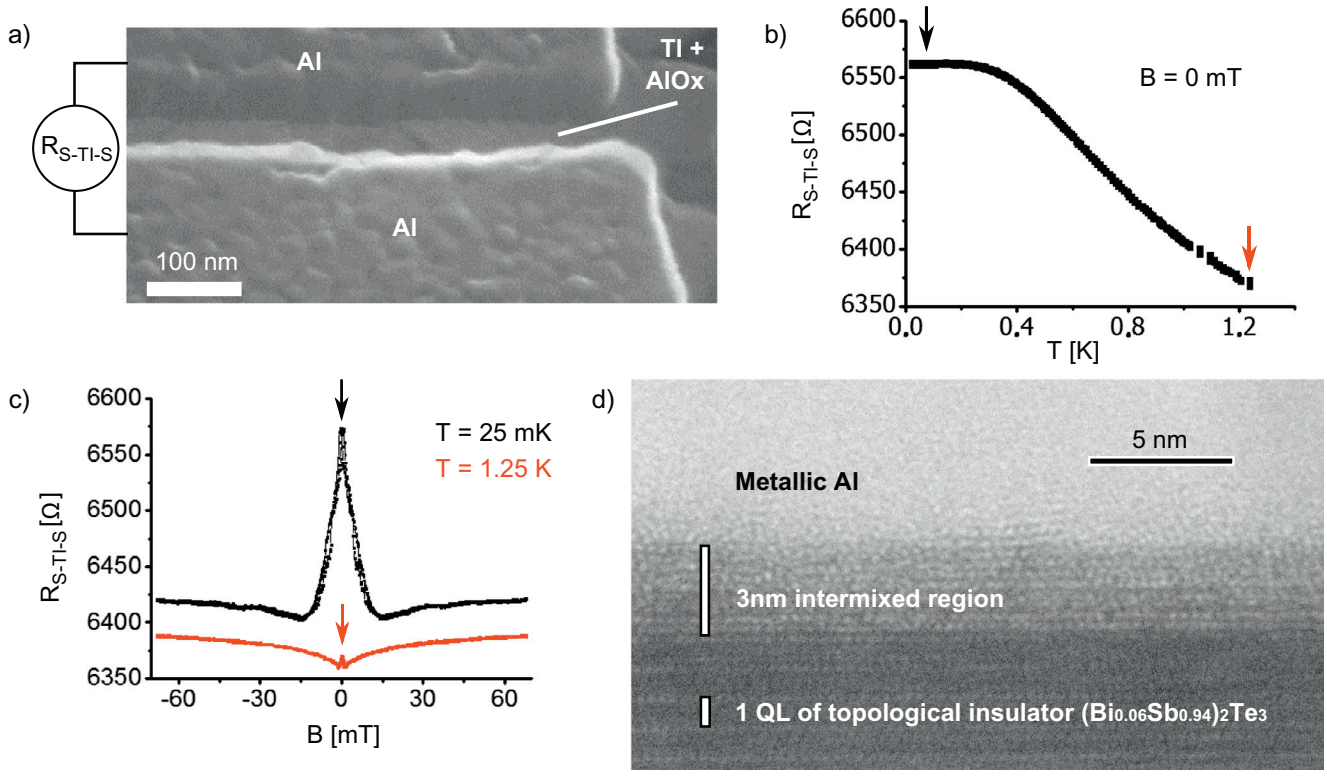

Fig. 3. Interface analysis. (a) Scanning electron micrograph of two Al-electrodes on top of a topological insulator forming a capped S-TI-S junction. (b) Resistance across the junction with respect to the temperature. (c) Differential resistance for small magnetic fields for 25 mK (black) and 1.25 K (red). (d) TEM image of the SC-TI interface. (For interpretation of the references to colour in this figure legend, the reader is referred to the web version of this article.)

has been improved, this approach paves the way towards scalable networks of topological hybrid devices.

5. Conclusion

To conclude, we created different shadow masks in the μm and nm range via focused ion beam patterning. Stencil lithography techniques allowed us to grow a protective AlO_x capping layer and spatially resolved metallic contacts on top of topological insulator thin films in one MBE session. Despite all samples being processed in-situ, transport measurements on a grown S-TI-S junction indicate a low transparency, due to a poor interface quality in between Al contacts and topological insulator thin film. TEM analysis confirms the existence of an intermixed region at the interface.

Author contributions

All authors have given approval to the final version of the manuscript.

Acknowledgement

Alexander Braginski is gratefully acknowledged for enlightening discussions. This work is supported by the German Science Foundation (DFG) under the priority program SPP1666 "Topological Insulators", as well as by the Helmholtz Association the "Virtual Institute for Topological Insulators" (VITI). Additionally this project has received funding from the European Union's Horizon 2020 research and innovation program under the ASCENT program, grant agreement No. 654384.

References

[1] L. Fu, C.L. Kane, E.J. Mele, Phys. Rev. Lett. 98 (2007) 106803.
[2] H. Zhang, C.-X. Liu, X.-L. Qi, X. Dai, Z. Fang, S.-C. Zhang, Nat. Phys. 5 (2009) 438.
[3] L. Fu, C. Kane, Phys. Rev. Lett. 100 (2008) 096407.
[4] J.E. Moore, Nature 464 (2010) 194.
[5] F. Hassler, 2014. Available from: arxiv:1404.0897.
[6] J. Wiedenmann, E. Bocquillon, R.S. Deacon, S. Hartinger, O. Herrmann, T.M. Klapwijk, L. Maier, C. Ames, C. Brüne, C. Gould, A. Oiwa, K. Ishibashi, S. Tarucha, H. Buhmann, L.W. Molenkamp, Nat. Commun. 7 (2016) 10303.
[7] E. Bocquillon, R.S. Deacon, J. Wiedenmann, P. Leubner, T.M. Klapwijk, C. Brüne, K. Ishibashi, H. Buhmann, M.W. Molenkamp, Nat. Nanotech. 12 (2017) 137–143.
[8] C. Brüne, C. Thienel, M. Stuiber, J. Böttcher, H. Buhmann, E.G. Novik, C. Liu, E.M. Hankiewicz, L.W. Molenkamp, Phys. Rev. X 4 (2014) 041045.
[9] M. Neupane, S.-Y. Xu, L.A. Wray, A. Petersen, R. Shankar, N. Alidoust, Chang Liu, A. Fedorov, H. Ji, J.M. Allred, Y.S. Hor, T.-R. Chang, H.-T. Jeng, H. Lin, A. Bansil, R. J. Cava, M.Z. Hasan, Phys. Rev. B 85 (2012) 235406.
[10] C. Weyrich, M. Drögeler, J. Kampmeier, M. Eschbach, G. Mussler, T. Merzenich, T. Stoica, I.E. Batov, J. Schubert, L. Plucinski, B. Beschoten, C.M. Schneider, C. Stampfer, D. Grützmacher, Th. Schäpers, J. Phys.: Condens. Matter 28 (2016) 49.
[11] Z. Ren, A. Taskin, S. Sasaki, K. Segawa, Y. Ando, Phys. Rev. B 82 (2010) 241306.
[12] N. Koirala, M. Brahlek, M. Salehi, L. Wu, J. Dai, J. Waugh, T. Nummy, M. Han, J. Moon, Y. Zhu, D. Dessau, W. Wu, N.P. Armitage, S. Oh, Nano Lett. 15 (12) (2015) 8245–8249.
[13] Y. Xu, I. Miotkowski, C. Liu, J. Tian, H. Nam, N. Alidoust, J. Hu, C. Shih, M.Z. Hasan, Y.P. Chen, Nat. Phys. 10 (2014) 956–963.
[14] M. Lang, L. He, F. Xiu, X. Yu, J. Tang, Y. Wang, X. Kou, W. Jiang, A.V. Fedorov, K.L. Wang, Nano Lett. 6 (2012) 295.
[15] P. Schüffelgen, D. Rosenbach, M. P. Stehno, M. Lanius, G. Mussler, S. Trellenkamp, Th. Schäpers, A. Brinkman, D. Grützmacher, unpublished results.
[16] J.B. Oostinga, L. Maier, P. Schüffelgen, D. Knott, C. Ames, C. Brüne, G. Tkachov, H. Buhmann, L.W. Molenkamp, Phys. Rev. X 3 (2013) 021007.
[17] P. Schüffelgen, D. Rosenbach, J. Kampmeier, G. Mussler, P. Ngabonziza, M. P. Stehno, Y. Pang, L. Lu, Th. Schäpers, A. Brinkman, D. Grützmacher, unpublished results.
[18] O. Vazquez-Mena, L. Gross, S. Xie, L.G. Villanueva, J. Brugger, Microelectron. Eng. 132 (2015) 236–254.
[19] J. Krumrain, G. Mussler, S. Borisova, T. Stoica, L. Plucinski, C.M. Schneider, D. Grützmacher, J. Cryst. Growth 324 (2011) 115.
[20] M. Lanius, J. Kampmeier, S. Kölling, G. Mussler, P.M. Koenraad, D. Grützmacher, J. Cryst. Growth 453 (2016) 158–162.

[21] J. Kellner, M. Eschbach, J. Kampmeier, M. Lanius, E. Mlynczak, G. Mussler, B. Holländer, L. Plucinski, M. Liebmann, D. Grützmacher, C.M. Schneider, M. Morgenstern, Appl. Phys. Lett. 107 (2015) 25.
[22] http://www.norcada.com/products/silicon-membranes/ (accessed: 15.03.2017).
[23] J. Wang, C. Chang, H. Li, K. He, D. Zhang, M. Singh, X. Ma, N. Samarth, M. Xie, Q. Xue, M.H.W. Chan, Phys. Rev. B 85 (2012) 045415.
[24] L. Plucinski, A. Herdt, S. Fahrendorf, G. Bihlmayer, G. Mussler, S. Döring, J. Kampmeier, F. Matthes, D.E. Bürgler, D. Grützmacher, S. Blügel, C.M. Schneider, J. Appl. Phys. 113 (2013) 5.
[25] P. Ngabonziza, R. Heimbuch, N. de Jong, R.A. Klaassen, M.P. Stehno, M. Snelder, A. Solmaz, S.V. Ramankutty, E. Frantzeskakis, E. van Heumen, G. Koster, M.S. Golden, H.J.W. Zandvliet, A. Brinkman, Phys. Rev. B 92 (2015) 035405.